Composite Structures 200 (2018) 874–885

Contents lists available at ScienceDirect

Composite Structures

journal homepage: www.elsevier.com/locate/compstruct

Time-dependent behavior of layered magneto-electro-elastic cylindrical shell with viscoelastic interlayer

Peng Wu[a,b], Chao Hu[a], Qing-Hua Qin[a,*]

[a] Research School of Engineering, Australian National University, Canberra, Australia
[b] College of Civil Engineering, Nanjing Tech University, Nanjing, China

ARTICLE INFO

Keywords:
Magneto-electro-elastic
Layered cylindrical shell
Viscoelastic interlayer
Pseudo-Stroh formalism
Laplace transformation

ABSTRACT

In this work, an analytical solution for layered magneto-electro-elastic (MEE) cylindrical shell adhesively bonded by viscoelastic interlayer is developed to predict its time-dependent mechanical, electric and magnetic behaviors. The viscoelastic characteristic of the interlayer is modelled by the standard linear solid model. Each MEE layer is governed by the equations of magneto-electro-elasticity. The imperfect electric conditions between adjacent MEE layers are also considered. Using the Pseudo-Stroh formalism, a general solution with unknown coefficients is derived for each MEE layer. The Laplace transformation is applied to the constitutive equations of the viscoelastic interlayer. The coefficients are determined by the surface conditions as well as the interface conditions. The present solution can be used as the benchmark to assess results from numerical approaches. It is shown that the finite element solution converges to the present one as the mesh density increases; however, the finite element method is time-consuming in mesh division and calculation. Finally, the effects of time, shell angle, interlayer thickness and imperfect electric coefficient on the mechanical, electric and magnetic behaviors are investigated.

1. Introduction

Smart materials with piezoelectric and/or piezomagnetic traits are successfully employed as sensors and actuators in different branches of engineering, including applications in structural health monitoring, vibration control, robotics, etc. Additionally, the smart layered system composed of piezoelectric and piezomagnetic materials can exhibit new characteristic known as magnetoelectric coupling effect [1]. The individual layers in a smart system are either sintered together, or bonded by adhesive [2]. If the bonding stiffness between layers is extremely high, a perfect bonding can be achieved. However, due to the manufacturing flaw or low stiffness of adhesive, the imperfect bonding between layers occurs inevitably. It is known that the adhesive usually possesses viscoelastic property in nature; therefore, the bonding stiffness in the layered system is time-dependent. Such a problem exists widely in practice and is worth to be investigated thoroughly.

It is noted that analytical solutions are very important in engineering analysis and design because they can be employed to access the accuracy of numerical solutions [3–5]. A review of the literature indicates that many analytical models have been developed for the analysis of smart layered system. Pan [6] presented an exact solution for the bending analysis of multilayer magneto-electro-elastic (MEE) plates using the Stroh formalism and propagator matrix method. Based on the first order shear deformation theory, Qin and Yu [7] solved the plane problem of a crack terminating at the interface of a bimaterial piezoelectrics by means of axial conjugate approach. Ke and Wang [8] investigated the free vibration of MEE nanoplates based on the nonlocal theory and Kirchhoff plate theory. In their study, the Hamilton's principle was used to obtain the natural frequencies of MEE nanoplates. By extending the Stroh formalism, Vel et al. [9] analyzed the mechanism regarding the bending of layered piezoelectric plates. Qin and Ye [10] presented thermolectroelastic solutions for describing internal bone remodeling process through dividing inhomogeneous circular cylindrical bones into layers. By employing the Mindlin plate theory, Liu et al. [11] dealt with the vibration of a sandwich plate composed of two piezoelectric faces and an elastic core with clamped edge. Based on the Euler nanobeam model and Timoshenko nanobeam model, the dispersion behavior of waves in the MEE nanobeams was studied by Ma et al. [12]. Wu and Lu [13] proposed a modified Pagano method to discuss the dynamic responses of functionally graded magneto-electro-elastic plates with free electric/magnetic potential and flux conditions. By the use of the nonlocal theory as well as the Kirchhoff plate theory, Ke et al. [14] tackled the free vibration of MEE nanoplates subjected to biaxial loadings, temperature rise, electric and magnetic potentials. Milazzo

* Corresponding author.
E-mail address: qinghua.qin@anu.edu.au (Q.-H. Qin).

https://doi.org/10.1016/j.compstruct.2018.05.115
Received 8 February 2018; Received in revised form 19 May 2018; Accepted 28 May 2018
Available online 29 May 2018

et al. [15] proposed an analytical solution to predict the transient performance of a MEE bimorph beam with steady electric and magnetic fields. By employing the nonlocal Love's shell theory, Ke et al. [16] analyzed the size-dependent vibration of embedded MEE cylindrical nanoshells, which incorporated effects of the small scale parameter and thermo-electro-magnetic loadings.

In the above studies, the adjacent members in the layered system are assumed to be perfectly bonded. For the imperfect bonding, the linear spring model is the most popular for the analysis of smart layered structures in literature. Jiang et al. [17] developed a new reverberation-ray matrix method for the wave propagation of layered MEE cylinder with imperfect interfaces. The bending and free vibration behaviors of layered piezoelectric beams with interfacial slip were investigated by Zhou et al. [18] through using the state-space method. By virtue of the complex variable method, Fang et al. [19] presented the theoretical model for the imperfect interaction between a piezoelectric screw dislocation and an interphase layer in piezoelectric solids. An exact solution for a laminated cylindrical shell with imperfect bonding with attached piezoelectric actuator under transverse loading was developed by Wang and Zhong [20] dependent on the pseudo-Stroh formalism. With the application of the dislocation method, Bayat et al. [21] derived an analytical solution to analyze the effect of multiple defects on the orthotropic strip with piezoelectric coating. By means of the asymptotic homogenization method, the static problem for heterogeneous piezoelectric composite with mechanical and electrical imperfect contact was dissected by López-Realpozo et al. [22]. The propagation of shear horizontal waves in layered MEE system with imperfect contact was studied by Otero et al. [23]. Moreover, Rodriguez-Ramos et al. [24] proposed an analytical model for piezoelectric composite reinforced by unidirectional fibers with interfacial imperfection.

Although the linear spring model is simple and easy to use, it can predict static interfacial bonding behavior only. It is noted from the literature that the viscoelastic property of adhesive can be properly simulated by the standard linear solid (SLS) model [25–29], which consists of a linear spring and a Maxwell unit in parallel, as shown in Fig. 1. To the best of our knowledge, no analytical solution for smart layered structures with SLS-model imperfect bonding has been reported yet. In this paper, an analytical model is presented for layered MEE cylindrical shell adhesively bonded by viscoelastic interlayer and subjected to radial load. The mechanical behavior of the interlayer is modeled by the SLS model, and the governing equations for each MEE layer are built upon the magneto-electro-elasticity theory. The imperfect electric conditions between adjacent MEE layers are also considered. Furthermore, the effects of the time, shell angle, interlayer thickness and imperfect electric coefficient on the mechanical, electric and magnetic behaviors are examined.

2. Analytical model

As shown in Fig. 2, a layered cylindrical shell is designed, whose internal radius is R_1, external radius R_2, thickness H, angle θ_0 and the length is infinite, consisting of p MEE layers with thickness h_i of layer i, adhesively bonded by thin viscoelastic interlayers with the same

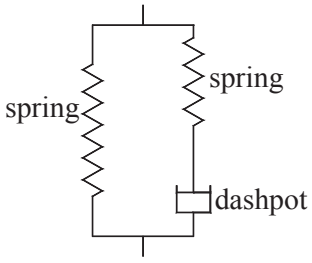

Fig. 1. Standard linear solid model.

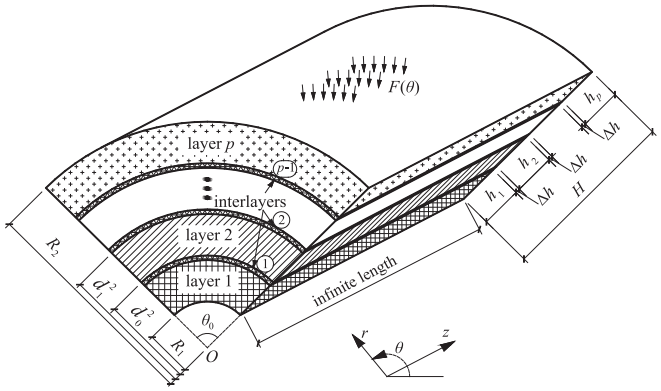

Fig. 2. Layered magneto-electro-elastic cylindrical shell with viscoelastic interlayers.

thickness Δh. A cylindrical coordinate system O-θrz is established to identify the location in the shell. Let d_0^i and d_1^i represent the distances from the internal and external surfaces of i-th MEE layer to the circle center O, respectively. The shell is simply supported and acted by a radial load $F(\theta)$ at the external surface. We deem the cylindrical shell in the state of generalized plane strain, which means the variables associated with stress, displacement, electric and magnetic fields are constant along z direction.

Further, the present study complies with four assumptions:

(1) The shell deformation is small and within the range of linearity.
(2) The adhesive interlayer is far thinner than the MEE layers, i.e. $\Delta h \ll h_i$.
(3) Based on the previous assumption, the interlayer displacement is assumed to be linearly distributed along the radial direction, which means the interlayer strain is constant through radial direction.
(4) The interlayer, made of adhesive, is relatively soft in comparison with the MEE layer; thus, its circumferential normal stress is negligible.

2.1. Stroh-type general solution for a MEE layer

The coupled constitutive equations for i-th MEE layer can be given in the tensor form [6,30]

$$\begin{aligned} &\sigma_j^i = c_{jk}^i\gamma_k^i - e_{kj}^i E_k^i - q_{kj}^i H_k^i, \\ &D_j^i = e_{jk}^i\gamma_k^i + \varepsilon_{jk}^i E_k^i + d_{jk}^i H_k^i, \\ &B_j^i = q_{jk}^i\gamma_k^i + d_{jk}^i E_k^i + \mu_{jk}^i H_k^i, \\ &i = 1, 2...p, \end{aligned} \tag{1}$$

where σ_j^i, γ_k^i, D_j^i, E_k^i, B_j^i, H_k^i are the stress, strain, electric displacement, electric field, magnetic induction and magnetic field, respectively; c_{jk}^i, e_{kj}^i, q_{kj}^i, ε_{jk}^i, d_{jk}^i, μ_{jk}^i are elastic, piezoelectric, piezo-magnetic, dielectric, magnetic-permeability and magneto-electric constants, respectively, whose details are given in Eq. (A1) of Appendix A. The general strain-displacement relations in generalized plane stain state are governed by [31]

$$\begin{aligned} &\varepsilon_\theta^i = \frac{u_r^i}{r} + \frac{1}{r}\frac{\partial u_\theta^i}{\partial\theta},\ \varepsilon_r^i = \frac{\partial u_r^i}{\partial r},\ \gamma_{rz}^i = \frac{\partial u_z^i}{\partial r},\ \gamma_{\theta z}^i = \frac{1}{r}\frac{\partial u_z^i}{\partial\theta}, \\ &\gamma_{r\theta}^i = \frac{1}{r}\frac{\partial u_r^i}{\partial\theta} + \frac{\partial u_\theta^i}{\partial r} - \frac{u_\theta^i}{r},\ E_\theta^i = -\frac{1}{r}\frac{\partial\phi^i}{\partial\theta},\ E_r^i = -\frac{\partial\phi^i}{\partial r}, \\ &H_\theta^i = -\frac{1}{r}\frac{\partial\psi^i}{\partial\theta},\ H_r^i = -\frac{\partial\psi^i}{\partial r},\ \varepsilon_z^i = E_z^i = H_z^i = 0, \\ &i = 1, 2, ...p, \end{aligned} \tag{2}$$

where u_θ^i, u_z^i, u_r^i are elastic displacement, and ϕ^i and ψ^i are electric and magnetic potentials, respectively. The equilibrium equations, in the absence of body forces, electric charge and current density, are given by [31]

$$\frac{\partial \sigma_r^i}{\partial r}+\frac{1}{r}\frac{\partial \tau_{r\theta}^i}{\partial \theta}+\frac{\sigma_r^i-\sigma_\theta^i}{r}=0,\quad \frac{\partial \tau_{r\theta}^i}{\partial r}+\frac{1}{r}\frac{\partial \sigma_\theta^i}{\partial \theta}+\frac{2\tau_{r\theta}^i}{r}=0,$$
$$\frac{\partial \tau_{rz}^i}{\partial r}+\frac{1}{r}\frac{\partial \tau_{\theta z}^i}{\partial \theta}+\frac{\tau_{rz}^i}{r}=0,\quad \frac{\partial D_r^i}{\partial r}+\frac{1}{r}\frac{\partial D_\theta^i}{\partial \theta}+\frac{D_r^i}{r}=0,$$
$$\frac{\partial B_r^i}{\partial r}+\frac{1}{r}\frac{\partial B_\theta^i}{\partial \theta}+\frac{B_r^i}{r}=0, i=1,2,...p. \tag{3}$$

The simply supported boundary condition can be expressed as

$$u_r^i=\phi^i=\psi^i=\sigma_\theta^i=\tau_{\theta z}^i=0, \text{ at } \theta=0,\ \theta_0,$$
$$i=1,\ 2,\ ...p, \tag{4}$$

With the boundary condition described in Eq. (4), the extended displacements, extended out-of-plane and extended in-plane stresses can be expanded into Fourier series, as follows

$$\begin{bmatrix} u_\theta^i(\theta,r,t)\\ u_z^i(\theta,r,t)\\ u_r^i(\theta,r,t)\\ \phi^i(\theta,r,t)\\ \psi^i(\theta,r,t)\end{bmatrix}=\sum_{m=1}^{\infty}\begin{bmatrix} u_{\theta,m}^i(r,t)\cos(\alpha_m\theta)\\ u_{z,m}^i(r,t)\sin(\alpha_m\theta)\\ u_{r,m}^i(r,t)\sin(\alpha_m\theta)\\ \phi_m^i(r,t)\sin(\alpha_m\theta)\\ \psi_m^i(r,t)\sin(\alpha_m\theta)\end{bmatrix},$$
$$\begin{bmatrix} \tau_{r\theta}^i(\theta,r,t)\\ \tau_{rz}^i(\theta,r,t)\\ \sigma_r^i(\theta,r,t)\\ D_r^i(\theta,r,t)\\ B_r^i(\theta,r,t)\end{bmatrix}=\sum_{m=1}^{\infty}\begin{bmatrix} \tau_{r\theta,m}^i(r,t)\cos(\alpha_m\theta)\\ \tau_{rz,m}^i(r,t)\sin(\alpha_m\theta)\\ \sigma_{r,m}^i(r,t)\sin(\alpha_m\theta)\\ D_{r,m}^i(r,t)\sin(\alpha_m\theta)\\ B_{r,m}^i(r,t)\sin(\alpha_m\theta)\end{bmatrix},$$
$$\begin{bmatrix} \sigma_\theta^i(\theta,r,t)\\ \sigma_z^i(\theta,r,t)\\ \tau_{\theta z}^i(\theta,r,t)\\ D_\theta^i(\theta,r,t)\\ D_z^i(\theta,r,t)\\ B_\theta^i(\theta,r,t)\\ B_z^i(\theta,r,t)\end{bmatrix}=\sum_{m=1}^{\infty}\begin{bmatrix} \sigma_{\theta,m}^i(r,t)\sin(\alpha_m\theta)\\ \sigma_{z,m}^i(r,t)\sin(\alpha_m\theta)\\ \tau_{\theta z,m}^i(r,t)\cos(\alpha_m\theta)\\ D_{\theta,m}^1(r,t)\cos(\alpha_m\theta)\\ D_{z,m}^1(r,t)\sin(\alpha_m\theta)\\ B_{\theta,m}^i(r,t)\cos(\alpha_m\theta)\\ B_{z,m}^i(r,t)\sin(\alpha_m\theta)\end{bmatrix},$$
$$i=1,\ 2,\ ...p. \tag{5}$$

where $\alpha_m=m\pi/\theta_0$. In view of the differential in Eqs. (2) and (3), the extended displacements and extended out-of-plane stresses are taken as the following form

$$\mathbf{D}_m^i(r,t)=r^{\lambda_m^i}\mathbf{a}_m^i(t),\quad \mathbf{O}_m^i(r,t)=r^{\lambda_m^i-1}\mathbf{b}_m^i(t), \tag{6}$$

where $\mathbf{a}_m^i(t)$ and $\mathbf{b}_m^i(t)$ are both column vectors containing 5 unknown coefficients associated with the time variable t, $i=1,2,...p$, $m=1,2,3,...$, and

$$\mathbf{D}_m^i(r,t)=[u_{\theta,m}^i(r,t)\ \ u_{z,m}^i(r,t)\ \ u_{r,m}^i(r,t)\ \ \phi_m^i(r,t)\ \ \psi_m^i(r,t)]^T,$$

$$\mathbf{O}_m^i(r,t)=[\tau_{r\theta,m}^i(r,t)\ \ \tau_{rz,m}^i(r,t)\ \ \sigma_{r,m}^i(r,t)\ \ D_{r,m}^i(r,t)\ \ B_{r,m}^i(r,t)]^T.$$

By substituting Eqs. (5) and (6) into Eqs. (1)–(3), two relations with respect to $\mathbf{a}_m^i(t)$ and $\mathbf{b}_m^i(t)$ are obtained

$$\mathbf{b}_m^i(t)=(-\mathbf{R}_{im}^T+\mathbf{T}_i\lambda_m^i)\mathbf{a}_m^i(t),$$
$$[\mathbf{Q}_{im}+(\mathbf{R}_{im}-\mathbf{R}_{im}^T)\lambda_m^i+\mathbf{T}_i(\lambda_m^i)^2]\mathbf{a}_m^i(t)=\mathbf{0},$$
$$i=1,\ 2...p,\ m=1,\ 2,\ 3..., \tag{7}$$

where

$$\mathbf{R}_{im}=\begin{bmatrix} c_{55}^i & 0 & \alpha_m c_{13}^i & \alpha_m e_{31}^i & \alpha_m q_{31}^i\\ 0 & 0 & 0 & 0 & 0\\ -\alpha_m c_{55}^i & 0 & -c_{13}^i & -e_{31}^i & -q_{31}^i\\ -\alpha_m e_{15}^i & 0 & 0 & 0 & 0\\ -\alpha_m q_{15}^i & 0 & 0 & 0 & 0\end{bmatrix},$$

$$\mathbf{T}_i=\begin{bmatrix} c_{55}^i & 0 & 0 & 0 & 0\\ 0 & c_{44}^i & 0 & 0 & 0\\ 0 & 0 & c_{33}^i & e_{33}^i & q_{33}^i\\ 0 & 0 & e_{33}^i & -\varepsilon_{33}^i & -d_{33}^i\\ 0 & 0 & q_{33}^i & -d_{33}^i & -\mu_{33}^i\end{bmatrix},$$

,

$$\mathbf{Q}_{im}=\begin{bmatrix} -(\alpha_m)^2c_{11}^i-c_{55}^i & 0 & \alpha_m(c_{11}^i+c_{55}^i) & \alpha_m e_{15}^i & \alpha_m q_{15}^i\\ 0 & -(\alpha_m)^2c_{66}^i & 0 & 0 & 0\\ \alpha_m(c_{11}^i+c_{55}^i) & 0 & -c_{11}^i-(\alpha_m)^2c_{55}^i & -(\alpha_m)^2e_{15}^i & -(\alpha_m)^2q_{15}^i\\ \alpha_m e_{15}^i & 0 & -(\alpha_m)^2e_{15}^i & (\alpha_m)^2\varepsilon_{11}^i & (\alpha_m)^2d_{11}^i\\ \alpha_m q_{15}^i & 0 & -(\alpha_m)^2q_{15}^i & (\alpha_m)^2d_{11}^i & (\alpha_m)^2\mu_{11}^i\end{bmatrix}.$$

The second equation in Eq. (7) can be recast into a standard eigenvalue equation, as follows [20,30]

$$\mathbf{N}_{im}\begin{bmatrix}\mathbf{a}_m^i(t)\\ \mathbf{b}_m^i(t)\end{bmatrix}=\lambda_m^i\begin{bmatrix}\mathbf{a}_m^i(t)\\ \mathbf{b}_m^i(t)\end{bmatrix},$$
$$i=1,\ 2...p,\ m=1,\ 2,\ 3..., \tag{8}$$

where

$$\mathbf{N}_{im}=\begin{bmatrix}\mathbf{T}_i^{-1}\mathbf{R}_{im}^T & \mathbf{T}_i^{-1}\\ -\mathbf{Q}_{im}-\mathbf{R}_{im}\mathbf{T}_i^{-1}\mathbf{R}_{im}^T & -\mathbf{R}_{im}\mathbf{T}_i^{-1}\end{bmatrix}.$$

Further, the general solution for the extended displacements and extended out-of-plane stresses is obtained

$$\begin{bmatrix}\mathbf{D}_m^i(r,t)\\ r\mathbf{O}_m^i(r,t)\end{bmatrix}=\mathbf{E}_m^i r^{\mathbf{B}_m^i}\mathbf{C}_m^i(t),$$
$$i=1,\ 2...p,\ m=1,\ 2,\ 3..., \tag{9}$$

where $\mathbf{B}_m^i$ is a diagonal matrix including 10 eigenvalues of Eq. (8), $\mathbf{E}_m^i$ is a matrix consisting of 10 corresponding eigenvectors, and $\mathbf{C}_m^i(t)$ is a column vector containing 10 unknown coefficients associated with t. We define

$$\mathbf{\Psi}_m^i(r)=\begin{bmatrix}\mathbf{W}_{im}^1(r)\\ \mathbf{W}_{im}^2(r)\end{bmatrix}=\begin{bmatrix} W_{im}^{1,1}(r) & W_{im}^{1,2}(r) & ... & W_{im}^{1,10}(r)\\ W_{im}^{2,1}(r) & W_{im}^{2,2}(r) & ... & W_{im}^{2,10}(r)\\ ... & ... & ... & ...\\ W_{im}^{10,1}(r) & W_{im}^{10,2}(r) & ... & W_{im}^{10,10}(r)\end{bmatrix}$$
$$=\mathbf{E}_m^i r^{\mathbf{B}_m^i},$$
$$i=1,\ 2...p,\ m=1,\ 2,\ 3..., \tag{10}$$

where $\mathbf{W}_{im}^1(r)$ and $\mathbf{W}_{im}^2(r)$ are both 5×10 sub-matrixes. By reusing Eqs. (1)–(3), the general solution for the extended in-plane stresses can be expressed by

Table 1
Material parameters of $BaTiO_3$ and $CoFe_2O_4$ [6].

$BaTiO_3$	$CoFe_2O_4$
$c_{11}^i = c_{22}^i = 166$, $c_{12}^i = 77$, $c_{13}^i = c_{23}^i = 78$, $c_{33}^i = 162$	$c_{11}^i = c_{22}^i = 286$, $c_{12}^i = 173$, $c_{13}^i = c_{23}^i = 170.5$
$c_{44}^i = c_{55}^i = 43$, $c_{66}^i = 44.5$	$c_{33}^i = 269.5$, $c_{44}^i = c_{55}^i = 45.3$, $c_{66}^i = 56.5$
$e_{31}^i = e_{32}^i = -4.4$, $e_{33}^i = 18.6$, $e_{24}^i = e_{15}^i = 11.6$	$q_{31}^i = q_{32}^i = 580.3$, $q_{33}^i = 699.7$, $q_{24}^i = q_{15}^i = 550$
$\varepsilon_{11}^i = \varepsilon_{22}^i = 11.2$, $\varepsilon_{33}^i = 12.6$	$\varepsilon_{11}^i = \varepsilon_{22}^i = 0.08$, $\varepsilon_{33}^i = 0.093$
$\mu_{11}^i = \mu_{22}^i = 5$, $\mu_{33}^i = 10$	$\mu_{11}^i = \mu_{22}^i = -590$, $\mu_{33}^i = 157$

Note: the units of material parameters are: c_{jk}^i in 10^9 N/m^2, e_{kj}^i in C/m^2, q_{kj}^i in N/(Am), ε_{jk}^i in 10^{-9} C^2/(Nm^2) and μ_{jk}^i in 10^{-6} Ns^2/C^2.

$$\begin{bmatrix}\sigma_{\theta,m}^i\\ \sigma_{z,m}^i\end{bmatrix} = \begin{bmatrix}c_{11}^i\\ c_{12}^i\end{bmatrix}\frac{u_{r,m}^i - \alpha_m u_{\theta,m}^i}{r}$$

$$+\begin{bmatrix}c_{13}^i & e_{31}^i & q_{31}^i\\ c_{23}^i & e_{32}^i & q_{32}^i\end{bmatrix}(\boldsymbol{\varkappa}^i)^{-1}\begin{bmatrix}\sigma_{r,m}^i - c_{13}^i\frac{u_{r,m}^i - \alpha_m u_{\theta,m}^i}{r}\\ D_{r,m}^i - e_{31}^i\frac{u_{r,m}^i - \alpha_m u_{\theta,m}^i}{r}\\ B_{r,m}^i - q_{31}^i\frac{u_{r,m}^i - \alpha_m u_{\theta,m}^i}{r}\end{bmatrix},$$

$$D_{\theta,m}^i = \frac{e_{15}^i}{c_{55}^i}\tau_{r\theta,m}^i - \alpha_m\left(\frac{e_{15}^i e_{15}^i}{c_{55}^i} + \varepsilon_{11}^i\right)\frac{\phi_m^i}{r}$$

$$-\alpha_m\left(\frac{e_{15}^i q_{15}^i}{c_{55}^i} + d_{11}^i\right)\frac{\psi_m^i}{r},$$

$$B_{\theta,m}^i = \frac{q_{15}^i}{c_{55}^i}\tau_{r\theta,m}^i - \alpha_m\left(\frac{e_{15}^i q_{15}^i}{c_{55}^i} + d_{11}^i\right)\frac{\phi_m^i}{r}$$

$$-\alpha_m\left(\frac{q_{15}^i q_{15}^i}{c_{55}^i} + \mu_{11}^i\right)\frac{\psi_m^i}{r},$$

$$\tau_{\theta z,m}^i = -\alpha_m c_{66}^i\frac{u_{z,m}^i}{r},\ D_{z,m}^i = \frac{e_{24}^i}{c_{44}^i}\tau_{rz,m}^i,\ B_{z,m}^i = \frac{q_{24}^i}{c_{44}^i}\tau_{rz,m}^i,$$

$$i = 1, 2...p,\ m = 1, 2, 3..., \tag{11}$$

where

$$\boldsymbol{\varkappa}^i = \begin{bmatrix}c_{33}^i & e_{33}^i & q_{33}^i\\ e_{33}^i & -\varepsilon_{33}^i & -d_{33}^i\\ q_{33}^i & -d_{33}^i & -\mu_{33}^i\end{bmatrix}.$$

2.2. Equations of an adhesive interlayer

By employing the SLS model, the shear modulus in the interlayer is given by

$$G^*(t) = G_1^* e^{-t/\theta_G^*} + G_2^*, \tag{12}$$

where the variables with superscript * belong to the interlayer, θ_G^* denotes the relaxation time, G_1^* the relaxation moduli and G_2^* the long-term moduli. These parameters can be measured through the creep test [32]. For simplicity, the Poisson's ratio of the interlayer μ^* is assumed to be time-independent. Therefore, the Young's modulus of the interlayer can be expressed by

$$E^*(t) = 2(1 + \mu^*)G^*(t). \tag{13}$$

According to the linear viscoelasticity theory [33], the constitutive equations for the interlayer are given by

$$\sigma_{r,m}^{*i}(t) = E^*(t)\varepsilon_{r,m}^{*i}(0) + \int_0^t E^{*i}(t-\xi)\frac{\partial\varepsilon_{r,m}^{*i}(\xi)}{\partial\xi}d\xi,$$

$$\tau_{r\theta,m}^{*i}(t) = G^*(t)\gamma_{r\theta,m}^{*i}(0) + \int_0^t G^{*i}(t-\xi)\frac{\partial\gamma_{r\theta,m}^{*i}(\xi)}{\partial\xi}d\xi,$$

$$\tau_{r\theta,m}^{*i}(t) = G^*(t)\gamma_{r\theta,m}^{*i}(0) + \int_0^t G^{*i}(t-\xi)\frac{\partial\gamma_{r\theta,m}^{*i}(\theta,\xi)}{\partial\xi}d\xi,$$

$$i = 1, 2...p,\ m = 1, 2, 3... \tag{14}$$

This equation indicates the memory effect of viscoelasticity, i.e., the stress at a time depends on not only the current strain but also the strain history. For briefness, Eq. (14) is then rewritten into the Stieltjes convolution form [34], as follows

$$\sigma_{r,m}^{*i}(t) = 2(1 + \mu^*)\varepsilon_{r,m}^{*i}(t) \otimes dG^*(t),$$

$$\tau_{r\theta,m}^{*i}(t) = \gamma_{r\theta,m}^{*i}(t) \otimes dG^*(t),$$

$$\tau_{rz,m}^{*i}(t) = \gamma_{rz,m}^{*i}(t) \otimes dG^*(t),\ i = 1, 2...p,\ m = 1, 2, 3..., \tag{15}$$

where the symbol $\otimes$ means the convolution operation. The stresses in the interlayer are in balance with those in the adjacent MEE layer, i.e.,

$$\sigma_{r,m}^{*i}(t) = \sigma_{r,m}^i(d_1^i, t) = \sigma_{r,m}^{i+1}(d_0^{i+1}, t),$$

$$\tau_{r\theta,m}^{*i}(t) = \tau_{r\theta,m}^{*i}(d_1^i, t) = \tau_{r\theta,m}^{*i+1}(d_0^{i+1}, t),$$

$$\tau_{rz,m}^{*i}(t) = \tau_{rz,m}^{*i}(d_1^i, t) = \tau_{rz,m}^{*i+1}(d_0^{i+1}, t),$$

$$i = 1, 2...p,\ m = 1, 2, 3... \tag{16}$$

Recalling the third assumption, the strains in the interlayer can be expressed as

$$\varepsilon_{r,m}^{*i}(t) = \frac{u_{r,m}^{i+1}(d_0^{i+1}, t) - u_{r,m}^i(d_1^i, t)}{\Delta h},$$

$$\gamma_{r\theta,m}^{*i}(t) = \frac{\alpha_m}{d_1^i}u_{r,m}^i(d_1^i, t) + \frac{u_{\theta,m}^{i+1}(d_0^{i+1}, t) - u_{\theta,m}^i(d_1^i, t)}{\Delta h}$$

$$-\frac{u_{\theta,m}^i(d_1^i, t)}{d_1^i},$$

$$\gamma_{rz,m}^{*i}(t) = \frac{u_{z,m}^{i+1}(d_0^{i+1}, t) - u_{z,m}^i(d_1^i, t)}{\Delta h},$$

$$i = 1, 2...p-1,\ m = 1, 2, 3... \tag{17}$$

The imperfect electric conditions between adjacent layers are also considered, which can be given by [35,36]

$$D_{r,m}^{i+1}(d_0^{i+1}, t) - D_{r,m}^i(d_1^i, t) = -\chi_1\left(\frac{\alpha_m}{d_1^i}\right)^2\phi_m^i(d_1^i, t),$$

$$\phi_m^{i+1}(d_0^{i+1}, t) - \phi_m^i(d_1^i, t) = -\chi_2 D_{r,m}^i(d_1^i, t),$$

$$i = 1, 2...p-1,\ m = 1, 2, 3.... \tag{18}$$

This equation means following three conditions: (i) weakly dielectrically conducting condition, i.e., $\chi_1 = 0$, $\chi_2 > 0$; (ii) highly dielectrically conducting condition, i.e., $\chi_1 > 0$, $\chi_2 = 0$; (iii) the unelectroded condition, i.e., $\chi_1 = \chi_2 = 0$.

Here, the magnetic conditions between layers are assumed to be perfect, i.e.,

$$B_{r,m}^{i+1}(d_0^{i+1}, t) - B_{r,m}^i(d_1^i, t) = 0,$$

$$\psi_m^{i+1}(d_0^{i+1}, t) - \psi_m^i(d_1^i, t) = 0,$$

$$i = 1, 2...p-1,\ m = 1, 2, 3... \tag{19}$$

2.3. Solution for the layered system

In view of Eq. (5), the applied load is also expanded into Fourier series, as follows

Table 2
Viscoelastic parameters of epoxy [28].

Relaxation moduli	Long-term moduli	Relaxation time	Poisson's ratio
$G_1^* = 562.2 \times 10^6$ N/m^2	$G_2^* = 31.03 \times 10^6$ N/m^2	$\theta_G^* = 68.04$ s	$\mu^* = 0.3$

Table 3
The present solution at $\theta = \pi/16$, $r = 1.1$ m when $t = 1000$ s with different series items $N = 1, 3, 5 \ldots 13$.

N	σ_θ^1	σ_z^1	σ_r^1	$\tau_{r\theta}^1$	D_θ^1	B_θ^1	u_r^1	ϕ^1	ψ^1
1	0.2674	1.057	0.4460	−7.974	−4.422	−1.251	−2.815	−3.280	6.878
3	−1.435	−5.302	−2.069	−8.109	−6.288	−1.350	−2.834	−3.376	6.696
5	−1.225	−4.103	−2.391	−8.215	−5.509	−1.373	−2.834	−3.417	6.721
7	−1.216	−4.152	−2.505	−8.204	−5.413	−1.361	−2.834	−3.415	6.730
9	−1.215	−4.126	−2.490	−8.204	−5.382	−1.369	−2.834	−3.415	6.735
11	−1.211	−4.104	−2.503	−8.201	−5.399	−1.374	−2.834	−3.416	6.733
13	−1.210	−4.101	−2.508	−8.202	−5.397	−1.370	−2.834	−3.416	6.731

Note: the units of the above variables are: σ_θ^1 and $\tau_{r\theta}^1$ in 10^{-1} N/m^2, σ_z^1 and σ_r^1 in 10^{-2} N/m^2, D_θ^1 in 10^{-11} C/(m^2), B_θ^1 in 10^{-10} Wb/(m^2), u_r^1 in 10^{-12} m, ϕ^1 in 10^{-3} V, and ψ^1 in 10^{-6} C/s.

$$F(\theta) = \sum_{m=1}^{\infty} q_m \sin(\alpha_m \theta), \tag{20}$$

where $q_m = \frac{2}{\theta_0}\int_0^{\theta_0} F(\theta)\sin(\alpha_m\theta)d\theta$. The conditions at the internal and external surfaces of the shell are given by

$$\begin{aligned}&\mathbf{O}_m^1(R_1, t) = [0 \;\; 0 \;\; 0 \;\; 0 \;\; 0]^T,\\ &\mathbf{O}_m^p(R_2, t) = [0 \;\; 0 \;\; q_m \;\; 0 \;\; 0]^T,\\ &m = 1, 2, 3. \ldots\end{aligned} \tag{21}$$

Meanwhile, the adjacent conditions of Eqs. (16)–(19) can be rearranged into the matrix form:

$$\frac{\mathbf{K}_m^i}{\Delta h}\begin{bmatrix}\mathbf{D}_m^i(d_1^i, t)\\ d_1^i\mathbf{O}_m^i(d_1^i, t)\end{bmatrix} + \frac{1}{\Delta h}\begin{bmatrix}\mathbf{D}_m^{i+1}(d_0^{i+1}, t)\\ d_0^{i+1}\mathbf{O}_m^{i+1}(d_0^{i+1}, t)\end{bmatrix} = \mathbf{\Delta}_{im}^*(t) \tag{22}$$

where the matrix $\mathbf{K}_m^i$ is defined in Eq. (A2) of Appendix A, $i = 1, 2 \ldots, p-1$, $m = 1, 2, 3 \ldots$ and

$$\mathbf{\Delta}_m^i(t) = [\gamma_{r\theta,m}^{*i}(t) \;\; \gamma_{rz,m}^{*i}(t) \;\; \varepsilon_{r,m}^{*i}(t) \;\; 0 \;\; 0 \;\; 0 \;\; 0 \;\; 0 \;\; 0 \;\; 0]^T.$$

By combining the surface conditions as well as the adjacent conditions, a matrix equation for the unknown coefficients are obtained, as follows

$$\mathbf{\Omega}_m\mathbf{X}_m(t) = \mathbf{G}_m,\ m = 1, 2, 3\ldots, \tag{23}$$

where the detail of $\mathbf{\Omega}_m$ is given in Eq. (A3) of Appendix A, and

$$\mathbf{X}_m(t) = \begin{bmatrix}\mathbf{C}_m^1(t)\\ \mathbf{C}_m^2(t)\\ \cdots\\ \mathbf{C}_m^p(t)\end{bmatrix},\ \mathbf{G}_m = \begin{bmatrix}\mathbf{\Delta}_m^1\\ \mathbf{\Delta}_m^2\\ \cdots\\ \mathbf{\Delta}_m^{p-1}\\ \mathbf{Q}_m\end{bmatrix},\ \mathbf{Q}_m = \begin{bmatrix}0\\ \cdots\\ 0\\ q_m\\ 0\\ 0\end{bmatrix},$$

in which, $\mathbf{0}_1$ is a 10×10 null matrix, and $\mathbf{0}_2$ is a 5×10 null matrix. By virtue of Cramer's law of linear equations, the unknown coefficients can be expressed by the interlayer strains as

$$\begin{aligned}X_m^\beta(t) = &\sum_{k=1}^{p-1}\left[\frac{|\mathbf{\Omega}_{m,\beta,k}^{(\theta)}|}{|\mathbf{\Omega}_m|}\gamma_{r\theta,m}^{*k}(t) + \frac{|\mathbf{\Omega}_{m,\beta,k}^{(z)}|}{|\mathbf{\Omega}_m|}\gamma_{rz,m}^{*k}(t)\right.\\ &\left. + \frac{|\mathbf{\Omega}_{m,\beta,k}^{(r)}|}{|\mathbf{\Omega}_m|}\varepsilon_{r,m}^{*k}(t)\right] + \frac{|\mathbf{\Omega}_{m,\beta}^{(q)}|}{|\mathbf{\Omega}_m|}q_m,\\ C_{im}^j(t) = &X_m^{10i-10+j}(t),\\ &i = 1, 2\ldots p,\ m = 1, 2, 3\ldots, \beta = 1, 2\ldots 10p,\ j = 1, 2\ldots 10,\end{aligned} \tag{24}$$

where X_m^β is the β-th element of $\mathbf{X}_m(t)$; C_{im}^j is the j-th element of $\mathbf{C}_m^i(t)$; $\mathbf{\Omega}_{m,\beta,k}^{(\theta)}$, $\mathbf{\Omega}_{m,\beta,k}^{(z)}$, $\mathbf{\Omega}_{m,\beta,k}^{(r)}$, and $\mathbf{\Omega}_{m,\beta}^{(q)}$ are obtained by replacing the β-th column of $\mathbf{\Omega}_m$ with the vector $\mathbf{B}_k^{(\theta)}$, $\mathbf{B}_k^{(z)}$, $\mathbf{B}_k^{(r)}$ and $\mathbf{B}^{(q)}$, respectively, in which,

$$\mathbf{B}_k^{(\theta)} = \left[\underbrace{0 \;\cdots\; 0}_{10k-10} \;\; 1 \;\; \underbrace{0 \;\cdots\; 0}_{10(p-k)+9}\right]^T,\ \mathbf{B}_k^{(z)} = \left[\underbrace{0 \;\cdots\; 0}_{10k-9} \;\; 1 \;\; \underbrace{0 \;\cdots\; 0}_{10(p-k)+8}\right]^T,$$

Table 4
Comparison of σ_0, τ_0, u_0 and ϕ_0 when $t = 1000$ s between the present solution and the FE solution.

FE solution with different ζ						Present solution
ζ	2	5	10	15	20	
σ_0 [N/m^2]	9.429	9.796	9.859	9.871	9.882	9.899
Error (%)	4.76	1.05	0.412	0.294	0.183	/
τ_0 [10^{-1} N/m^2]	−1.888	−1.897	−1.903	−1.906	−1.907	−1.914
Error (%)	1.37	0.892	0.581	0.406	0.353	/
u_0 [10^{-11} m]	−4.988	−5.062	−5.101	−5.120	−5.127	−5.141
Error (%)	2.97	1.54	0.782	0.416	0.267	/
ϕ_0 [10^{-3} V]	−4.122	−4.004	−3.948	−3.912	−3.896	−3.887
Error (%)	6.05	3.01	1.56	0.632	0.242	/

Note: the error is calculated by |(FE-present)/present|.

$$\mathbf{B}_k^{(r)} = \left[\underbrace{0 \;\cdots\; 0}_{10k-8} \;\; 1 \;\; \underbrace{0 \;\cdots\; 0}_{10(p-k)+7}\right]^T,\ \mathbf{B}^{(q)} = \left[\underbrace{0 \;\cdots\; 0}_{10p-3} \;\; 1 \;\; 0 \;\; 0\right]^T$$

.

By conducting Laplace transformation to Eqs. (12) and (15), one obtains

$$\begin{aligned}&\widehat{G}^*(s) = \frac{G_1^*}{s + 1/\theta_G^*} + \frac{G_2^*}{s},\\ &\hat{\tau}_{r\theta,m}^i(d_i^1, s) = \hat{\gamma}_{r\theta,m}^{*i}(s)s\widehat{G}^*(s),\\ &\hat{\tau}_{rz,m}^i(d_i^1, s) = \hat{\gamma}_{rz,m}^{*i}(s)s\widehat{G}^*(s),\\ &\hat{\sigma}_{r,m}^i(d_i^1, s) = 2(1+\mu^*)\hat{\varepsilon}_r^{*i}(s)s\widehat{G}^*(s),\\ &i = 1, 2\ldots p-1,\ m = 1, 2, 3\ldots,\end{aligned} \tag{25}$$

where the variable with an over hat accent represents that it is in Laplace transformation shape. By substituting Eq. (24) into Eq. (9) and then substituting the results into Eq. (25), the equations for the interlayer strains are obtained

$$\left(\mathbf{A}_m + \mathbf{I}\frac{s}{s + 1/\theta_G^*}\right)\widehat{P}_m(s) = \frac{1}{s}\mathbf{H}_m,\quad m = 1, 2, 3\ldots, \tag{26}$$

where $\mathbf{I}$ is the unit matrix, the details of $\mathbf{A}_m$ and $\mathbf{H}_m$ are given in Eq. (A2) of Appendix A, and

$$\begin{aligned}&\widehat{P}_m(s) = [\hat{\gamma}_{r\theta,m}^{*1}(s)\ldots\hat{\gamma}_{r\theta,m}^{*(p-1)}(s)\\ &\hat{\gamma}_{rz}^{*1}(s)\ldots\hat{\gamma}_{rz}^{*(p-1)}(s) \;\; \hat{\varepsilon}_{r,m}^{*1}(s)\ldots\hat{\varepsilon}_{r,m}^{*(p-1)}(s)]^T.\end{aligned}$$

By reusing the Cramer's law of linear equations, the solution of interlayer strains in Laplace transformation shape is obtained

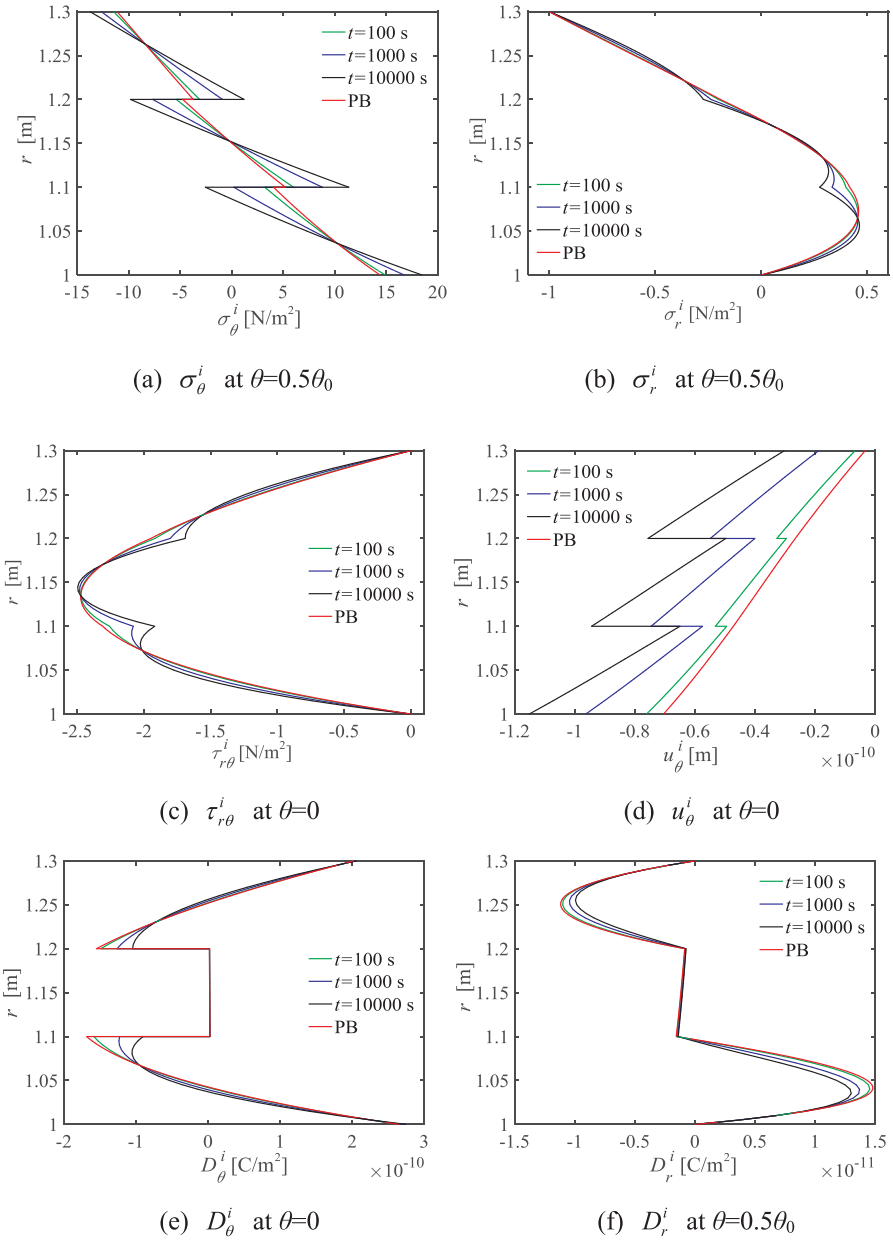

(a) σ_θ^i at θ=0.5θ_0 (b) σ_r^i at θ=0.5θ_0

(c) $\tau_{r\theta}^i$ at θ=0 (d) u_θ^i at θ=0

(e) D_θ^i at θ=0 (f) D_r^i at θ=0.5θ_0

Fig. 3. Distributions of the present solution along the radial direction at different time (PB means the perfectly bonded condition).

$$\widehat{P}_m^j(s) = \frac{\sum_{k=0}^{3p-3} \omega_{k,m}^j s^k}{\sum_{k=0}^{3p-3} \eta_{k,m} s^{k+1}},\ \widehat{\gamma}_{r\theta,m}^{*i}(s) = \widehat{P}_m^i(s),$$
$$\widehat{\gamma}_{rz,m}^{*i}(s) = \widehat{P}_m^{p-1+i}(s),\ \widehat{\varepsilon}_{r,m}^{*i}(s) = \widehat{P}_m^{2p-2+i}(s),$$
$$m = 1, 2, 3...,j = 1, 2...3(p-1), i = 1, 2...p-1, \tag{27}$$

where $\widehat{P}_m^j(s)$ is the j-th element of $\widehat{P}_m(s)$, and

$$\omega_{k,m}^j = \begin{cases} \sum_{n=0}^{k} [L_{m,n}^j C_{3p-3-n}^{3p-3-k} (1/\theta_G^*)^{3p-3-k}], & 0 \leqslant k \leqslant 3p-4, \\ \sum_{n=0}^{3p-4} L_{m,n}^j, & k = 3p-3, \end{cases}$$

$$\eta_{k,m} = \sum_{n=0}^{k} J_{m,n} C_{3p-3-n}^{3p-3-k} (1/\theta_G^*)^{3p-3-k},$$

in which, $C_a^b = \frac{a!}{b!(a-b)!}$; according to the permutation and combination theory, if arbitrary n columns in the determinant $|\mathbf{A}_m|$ are replaced by the same columns of $\mathbf{I}$, there will be C_{3p-3}^n kinds of results, and $J_{m,n}$ is the sum of all results. An example for $J_{m,n}$ is given in Appendix B. Let us define that $|\mathbf{A}_m^j|$ is the result that the j-th column of $|\mathbf{A}_m|$ is replaced by the column vector $\mathbf{H}_m$. If arbitrary n columns of $|\mathbf{A}_m^j|$, except for j-th column, are replaced by the same columns of $\mathbf{I}$, there will be C_{3p-4}^n kinds of results, and $L_{m,n}^j$ is the sum of all results. An example for $L_{m,n}^j$ is given in Appendix B. The inversed Laplace transformation of Eq. (27) is

$$P_m^j(t) = \sum_{l=1}^{3p-2} r_{l,m}^j e^{-s_{l,m}t},\ \gamma_{r\theta,m}^{*i}(t) = \frown P_m^i(t),$$
$$\gamma_{rz,m}^{*i}(t) = P_m^{p-1+i}(t),\ \ \varepsilon_{r,m}^{*i}(t) = P_m^{2p-2+i}(t),$$
$$m = 1, 2, 3..., j = 1, 2...3(p-1),\ \ i = 1, 2...p-1, \tag{28}$$

where $s_{l,m}$ (l = 1,2…3p − 2) is the root of the function of s: $\sum_{k=0}^{3p-3} \eta_{k,m} s^{k+1} = 0$, and

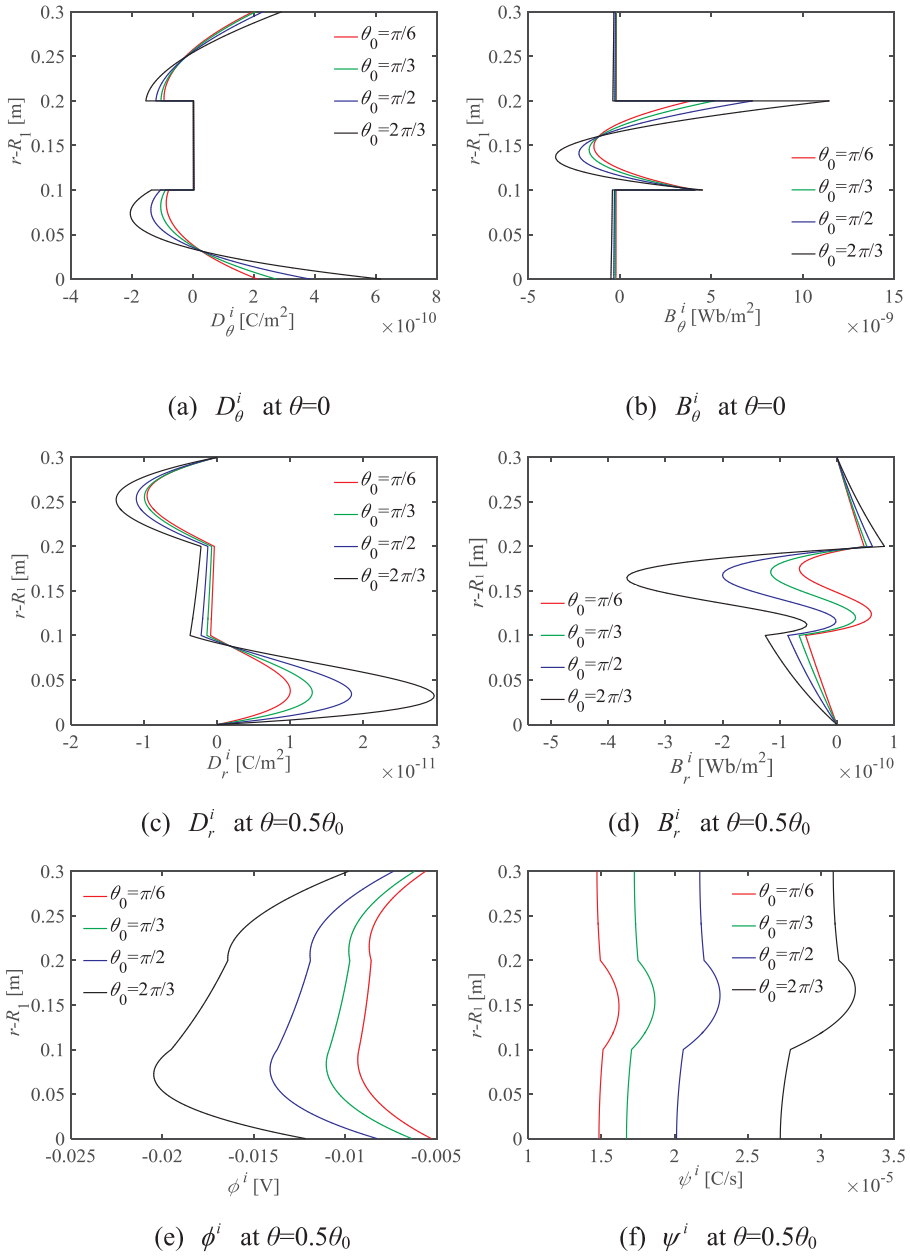

(a) D_θ^i at θ=0 (b) B_θ^i at θ=0

(c) D_r^i at θ=0.5θ_0 (d) B_r^i at θ=0.5θ_0

(e) ϕ^i at θ=0.5θ_0 (f) ψ^i at θ=0.5θ_0

Fig. 4. Radial distributions of electric and magnetic variables for different θ_0.

$$r_{l,m}^j = \frac{\sum_{k=0}^{3p-3} \omega_{k,m}^j (s_{l,m})^k}{\sum_{k=0}^{3p-3} (k+1)\eta_{k,m}(s_{l,m})^k}.$$

By substituting Eq. (28) into Eq. (24), the coefficients $\mathbf{C}_m^i(t)$ are determined. Finally, the solution for each MEE layer is obtained by substituting $\mathbf{C}_m^i(t)$ into Eq. (9).

It should be mentioned that the present method can also be applied to other boundary conditions. For example, the clamped boundary condition can be equivalent to a simply supported one acted by a distributed load at the edge which can be further determined by the zero displacement condition at the clamped edge [37].

3. Numerical examples

In the following example, the material parameters of piezoelectric $BaTiO_3$, magnetostrictive $CoFe_2O_4$ and viscoelastic epoxy are listed in Tables 1 and 2. Let us beforehand define six variables: $\sigma_0 = \sigma_\theta^1$ at $\theta = 0.5\theta$, $r = R_1$; $\tau_0 = \tau_{r\theta}^1$ at $\theta = 0$, $r = d_1^1$; $u_0 = u_r^1$ at $\theta = 0.5\theta$, $r = R_1$; $\phi_0 = \phi^1$ at $\theta = 0.5\theta$, $r = R_1$; $D_0 = D_\theta^1$ at $\theta = 0$, $r = d_1^1$; $B_0 = B_\theta^1$ at $\theta = 0$, $r = d_1^1$.

3.1. Verification of the solution

Since the present solution is expressed in series form, its convergence property is to be examined first. The infinite series in the solution are truncated up to finite ones, i.e., m = 1,2…N. Consider a simply supported three-layer cylindrical shell acted by a uniform load with $F(\theta) = 1\,\mathrm{N/m^2}$. The face and core layers in the shell are made of $BaTiO_3$ and $CoFe_2O_4$, respectively, which are bonded together by epoxy. The dimensions of the shell are $R_1 = 1$ m, $\theta_0 = 0.25\pi$, $h_1 = h_3 = 0.1$ m, $h_2 = 0.2$ m, $\Delta h = 2 \times 10^{-4}$ m. The electric condition between adjacent layers is unelectroded, i.e., $\chi_1 = \chi_2 = 0$. The present

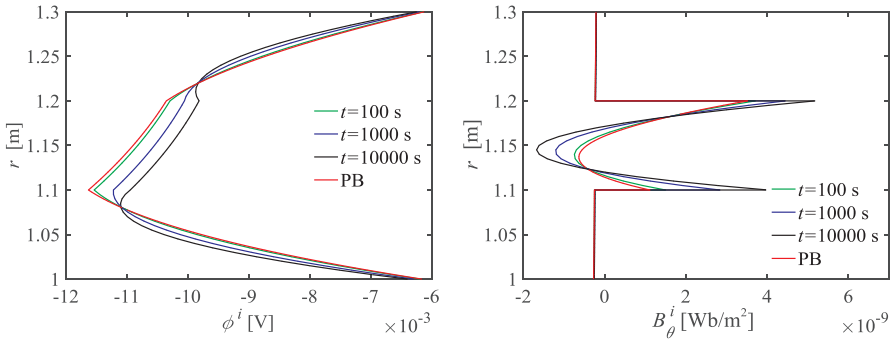

(g) ϕ^i at θ=0.5θ_0 (h) B_θ^i at θ=0

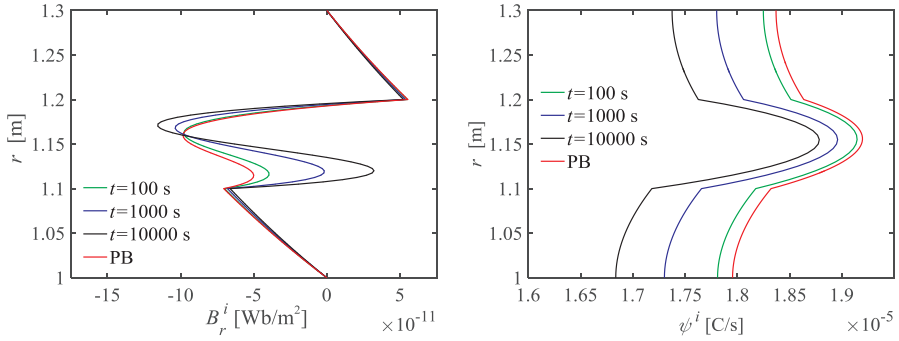

(i) B_r^i at θ=0.5θ_0 (j) ψ^i at θ=0.5θ_0

Fig. 4. (*continued*)

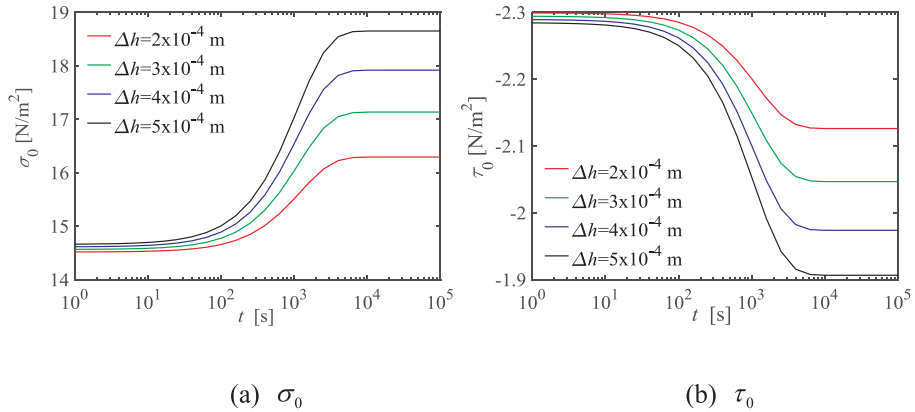

(a) σ_0 (b) τ_0

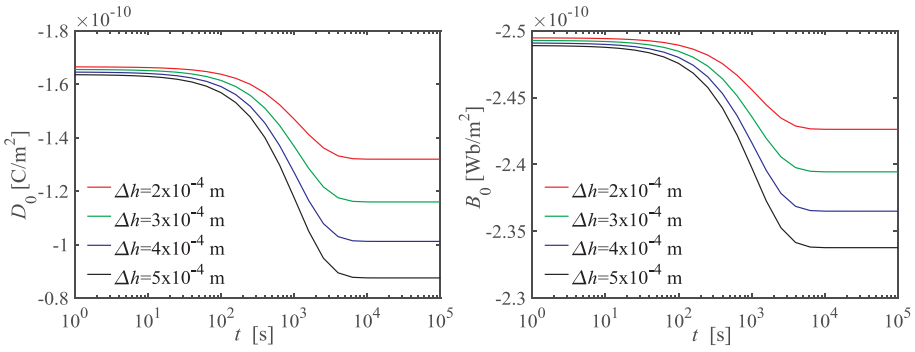

(c) D_0 (d) B_0

Fig. 5. Variations of σ_0, τ_0, D_0 and B_0 with respect to time for different Δh.

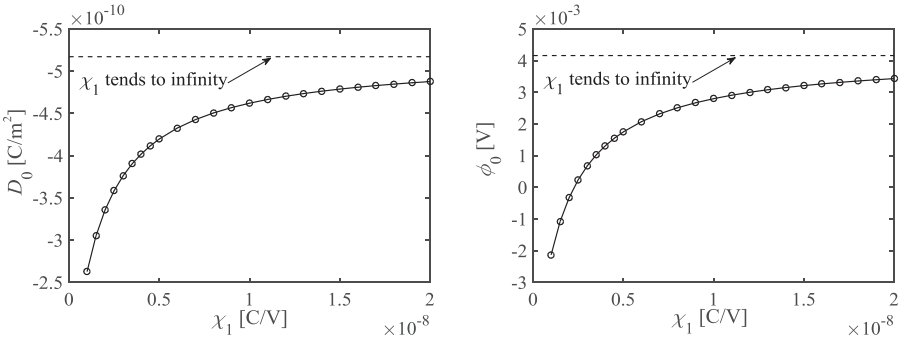

(a) D_0 (b) ϕ_0

Fig. 6. Variations of D_0 and ϕ_0 with respect to χ_1.

solution with different series items when $t = 1000$ s are given in Table 3. It is found that the present solution is rapidly convergent to the desired value along with an increase in N, and the extended displacements converge faster than the extended stresses. Besides, the present solution has higher convergence precision with at least three significant digits when $N = 13$.

The present solution is then compared with the solution obtained by the finite element (FE) software ANSYS. Since ANSYS cannot directly model the MEE material, we here consider a simply supported two-layer shell composed of two piezoelectric $BaTiO_3$ layers bonded by epoxy under uniform load $F(\theta) = 1\,\mathrm{N/m^2}$. The electric condition between adjacent MEE layers is insulating, i.e., $\chi_1 = 0$, $\chi_2 \to +\infty$ [36]. Other parameters are fixed at $R_1 = 1$ m, $\theta_0 = 0.25\pi$, $h_1 = 0.1$ m, $h_2 = 0.2$ m, $\Delta h = 2 \times 10^{-4}$ m. In the FE modeling, the $BaTiO_3$ layers and epoxy interlayer are respectively simulated by PLANE-13 and PLANE-182 elements with two-dimensional mesh. The thicknesses of the interlayer, internal and external layers are divided into 1, ζ and 2ζ elements, respectively, while the arc length of each layer is divided into 5ζ elements. The FE solution of σ_0, τ_0, u_0 and ϕ_0 when $t = 1000$ s for different ζ are compared with the present solution, as given in Table 4. It can be found that the FE solution tends to approach to the present one along with the increase of ζ. The FE solution agrees well with the present solution when $\zeta = 20$. However, the FE method is computationally expensive in mesh division and calculation when ζ is large.

3.2. Parameter study

Consider a simply supported three-layer shell formed by two piezoelectric $BaTiO_3$ face layers and a magnetostrictive $CoFe_2O_4$ core layer, bonded together by epoxy, and subjected to sinusoidal load $F(\theta) = \sin(\pi\theta/\theta_0)\,\mathrm{N/m^2}$. Let S_a represent the average arc length of the shell, i.e., $S_a = \theta_0(R_1 + 0.5H)$. The parameters are taken as $S_a = 1.2$ m, $h_1 = h_2 = h_3 = 0.1$ m, $\chi_2 = 0$, while t, θ_0, Δh and χ_1 are variable. In the following, the symbol $|.|$ means the absolute value of the variable.

The radial distributions of the present solution at different time with $\theta_0 = \pi/3$, $\Delta h = 5 \times 10^{-4}$ m, and $\chi_1 = 0$ are shown in Fig. 3, in which PB means the perfectly bonded condition, i.e., the extended displacements are continuous along the radial direction. It is found from Fig. 3 that: (i) the maximum of $|\sigma_\theta^i|$ and $|u_\theta^i|$ in each layer increases with the time; (ii) σ_r^i, $|\tau_{r\theta}^i|$ and $|D_\theta^i|$ near the interlayer decrease with the time, while $|B_\theta^i|$ near the interlayer increases with the time; (iii) D_θ^i, D_r^i in the magnetostrictive layer and B_θ^i, B_r^i in the piezoelectric layers are almost invariant with the time; (iv) the peak values of $|B_\theta^i|$ and $|B_r^i|$ increases with the time, while that of $|D_r^i|$ decreases with the time; (v) $|\phi^i|$ in the magnetostrictive layer and $|\psi^i|$ in each layer decrease with the time; (vi) the results in PB condition has considerable difference from those with the viscoelastic interlayer.

The radial distributions of electric and magnetic variables for different shell angle θ_0 with $\Delta h = 5 \times 10^{-4}$ m, $\chi_1 = 0$, $t = 1000$ s are shown in Fig. 4. It is found from Fig. 4 that: (i) $|D_\theta^i|$ near the surfaces of piezoelectric layers increases as θ_0 increases; (ii) the peak value of $|D_r^i|$ in the piezoelectric layers and those of $|B_\theta^i|$ and $|B_r^i|$ in the magnetostrictive layer increase as θ_0 increases; (iii) $|\phi^i|$ and $|\psi^i|$ in each layer increase as θ_0 increases.

Fig. 5 demonstrates the effect of interlayer thickness Δh on the variations of σ_0, τ_0, D_0 and B_0 with respect to time when $\chi_1 = 0$, $\theta_0 = \pi/3$. It is noted from Fig. 5 that: (i) $|\sigma_0|$ increases with the time, while $|\tau_0|$, $|D_0|$ and $|B_0|$ decrease with the time; (ii) they all tends to be constant after $t = 10^4$ s; (iii) $|\sigma_0|$ increases as Δh increases, while $|\tau_0|$, $|D_0|$ and $|B_0|$ decrease as Δh increases.

The variations of D_0 and ϕ_0 with respect to χ_1 when $\theta_0 = \pi/3$, $\Delta h = 5 \times 10^{-4}$ m, $t = 1000$ s are given in Fig. 6. It can be found from Fig. 6 that $|D_0|$ and ϕ_0 increase as χ_1 increases. They tend to be constant when χ_1 approaches infinity.

4. Conclusions

Analytical solution for layered MEE cylindrical shell with viscoelastic interlayer subjected to a radial load is developed to study the time-varying behavior in the shell. The results obtained from the above analysis can be boiled down to following conclusions:

(1) The present solution in the form of Fourier series has rapid convergence speed and high convergence precision.
(2) The FE result with small mesh size is in good agreement with the present one, but the FE method is time-consuming in mesh division and computation.
(3) The mechanical, electric and magnetic variables in the shell vary with the time; however, they tend to be constant after a certain time.
(4) The shell angle has effect on the electric and magnetic variables. The absolute values of electric and magnetic potentials in the shell increase as the shell angle increases.
(5) The circumferential normal stress increases as the interlayer thickness increases, while the shear stress, electric displacement, magnetic induction near the interlayer decrease as the interlayer thickness increases.
(6) The electric potential and the absolute value of electric displacement increase and tend to be constant as the imperfect coefficient increases.

Acknowledgements

The authors are grateful for the financial support received from the Nature Science Foundation of China (Grant No. 11772204) and Australian Research Council (Grant No. DP160102491).

Appendix A

The tensors in Eq. (1) are defined as follows:

$$[\sigma^i] = [\sigma_\theta^i \ \ \sigma_z^i \ \ \sigma_r^i \ \ \tau_{rz}^i \ \ \tau_{r\theta}^i \ \ \tau_{\theta z}^i]^T,$$

$$[\gamma^i] = [\varepsilon_\theta^i \ \ \varepsilon_z^i \ \ \varepsilon_r^i \ \ \gamma_{rz}^i \ \ \gamma_{r\theta}^i \ \ \gamma_{\theta z}^i]^T,$$

$$[D^i] = [D_\theta^i \ \ D_z^i \ \ D_r^i]^T, \ [E^i] = [E_\theta^i \ \ E_z^i \ \ E_r^i]^T,$$

$$[B^i] = [B_\theta^i \ \ B_z^i \ \ B_r^i]^T, \ [H^i] = \left[H_\theta^i \ \ H_z^i \ \ H_r^i\right]^T,$$

$$[c^i] = \begin{bmatrix} c_{11}^i & c_{12}^i & c_{13}^i & 0 & 0 & 0 \\ & c_{22}^i & c_{23}^i & 0 & 0 & 0 \\ & & c_{33}^i & 0 & 0 & 0 \\ & & & c_{44}^i & 0 & 0 \\ & sym. & & & c_{55}^i & 0 \\ & & & & & c_{66}^i \end{bmatrix},$$

$$[e^i] = \begin{bmatrix} 0 & 0 & e_{31}^i \\ 0 & 0 & e_{32}^i \\ 0 & 0 & e_{33}^i \\ 0 & e_{24}^i & 0 \\ e_{15}^i & 0 & 0 \\ 0 & 0 & 0 \end{bmatrix},$$

$$[q^i] = \begin{bmatrix} 0 & 0 & q_{31}^i \\ 0 & 0 & q_{32}^i \\ 0 & 0 & q_{33}^i \\ 0 & q_{24}^i & 0 \\ q_{15}^i & 0 & 0 \\ 0 & 0 & 0 \end{bmatrix},$$

$$[\varepsilon^i] = \begin{bmatrix} \varepsilon_{11}^i & 0 & 0 \\ 0 & \varepsilon_{22}^i & 0 \\ 0 & 0 & \varepsilon_{33}^i \end{bmatrix}, \ [d^i] = \begin{bmatrix} d_{11}^i & 0 & 0 \\ 0 & d_{22}^i & 0 \\ 0 & 0 & d_{33}^i \end{bmatrix},$$

$$[\mu^i] = \begin{bmatrix} \mu_{11}^i & 0 & 0 \\ 0 & \mu_{22}^i & 0 \\ 0 & 0 & \mu_{33}^i \end{bmatrix} \tag{A1}$$

The matrixes $\mathbf{K}_m^i$ in Eq. (22) and $\mathbf{\Omega}_m$ in Eq. (23) are defined as following

$$\mathbf{K}_m^i = \begin{bmatrix} -1-\frac{\Delta h}{d_1^i} & 0 & \frac{\Delta h \alpha_m}{d_1^i} & 0 & 0 & 0 & 0 & 0 & 0 & 0 \\ 0 & -1 & 0 & 0 & 0 & 0 & 0 & 0 & 0 & 0 \\ 0 & 0 & -1 & 0 & 0 & 0 & 0 & 0 & 0 & 0 \\ 0 & 0 & 0 & -1 & 0 & 0 & 0 & 0 & \frac{\chi_2}{d_1^i} & 0 \\ 0 & 0 & 0 & 0 & -1 & 0 & 0 & 0 & 0 & 0 \\ 0 & 0 & 0 & 0 & 0 & -1 & 0 & 0 & 0 & 0 \\ 0 & 0 & 0 & 0 & 0 & 0 & -1 & 0 & 0 & 0 \\ 0 & 0 & 0 & 0 & 0 & 0 & 0 & -1 & 0 & 0 \\ 0 & 0 & 0 & \frac{\chi_1(\alpha_m)^2}{d_1^i} & 0 & 0 & 0 & 0 & -1 & 0 \\ 0 & 0 & 0 & 0 & 0 & 0 & 0 & 0 & 0 & -1 \end{bmatrix}, \tag{A2}$$

$$\mathbf{\Omega}_m = \begin{bmatrix} \frac{\mathbf{K}_m^1}{\Delta h}\mathbf{\Psi}_m^1(d_1^1) & \frac{1}{\Delta h}\mathbf{\Psi}_m^2(d_0^2) & \mathbf{0}_1 & \cdots & \cdots & \cdots \\ \mathbf{0}_1 & \frac{\mathbf{K}_m^2}{\Delta h}\mathbf{\Psi}_m^2(d_1^2) & \frac{1}{\Delta h}\mathbf{\Psi}_m^3(d_0^3) & \mathbf{0}_1 & & \cdots \\ & & \cdots & \cdots & & \\ \cdots & \mathbf{0}_1 & \frac{\mathbf{K}_m^i}{\Delta h}\mathbf{\Psi}_m^i(d_1^i) & \frac{1}{\Delta h}\mathbf{\Psi}_m^{i+1}(d_0^{i+1}) & \mathbf{0}_1 & \\ & & \cdots & \cdots & & \\ \cdots & \cdots & \mathbf{0}_1 & \frac{\mathbf{K}_m^{p-1}}{\Delta h}\mathbf{\Psi}_m^{p-1}(d_1^{p-1}) & \frac{1}{\Delta h}\mathbf{\Psi}_m^p(d_0^p) & \\ \mathbf{M}_m^1 & \mathbf{0}_1 & \cdots & \mathbf{0}_1 & \mathbf{M}_m^p & \end{bmatrix}, \tag{A3}$$

where

$$\mathbf{M}_m^1 = \frac{1}{R_1}\begin{bmatrix}\mathbf{W}_{1m}^2(R_1)\\ \mathbf{0}_2\end{bmatrix},\ \mathbf{M}_m^p = \frac{1}{R_2}\begin{bmatrix}\mathbf{0}_2\\ \mathbf{W}_{pm}^2(R_2)\end{bmatrix}.$$

The details of matrixes $\mathbf{A}_m$ and $\mathbf{H}_m$ in Eq. (26) are given by

$$\mathbf{A}_m = \begin{bmatrix}\mathbf{A}_m^{11} & \mathbf{A}_m^{12} & \mathbf{A}_m^{13}\\ \mathbf{A}_m^{21} & \mathbf{A}_m^{22} & \mathbf{A}_m^{23}\\ \mathbf{A}_m^{31} & \mathbf{A}_m^{32} & \mathbf{A}_m^{33}\end{bmatrix},\ \mathbf{H}_m = \begin{bmatrix}\mathbf{H}_m^1\\ \mathbf{H}_m^2\\ \mathbf{H}_m^3\end{bmatrix},$$

$$\mathbf{A}_m^{11}(i,k) = -\frac{1}{d_i^1 G_1^*}\sum_{j=1}^{10} W_{im}^{6,j}(d_i^1)\frac{\left|\mathbf{\Omega}_{m,10i-10+j,k}^{(\theta)}\right|}{|\mathbf{\Omega}_m|} + \delta_{ik}\frac{G_2^*}{G_1^*},$$

$$\mathbf{A}_m^{12}(i,k) = -\frac{1}{d_i^1 G_1^*}\sum_{j=1}^{10} W_{im}^{6,j}(d_i^1)\frac{\left|\mathbf{\Omega}_{m,10i-10+j,k}^{(z)}\right|}{|\mathbf{\Omega}_m|},$$

$$\mathbf{A}_m^{13}(i,k) = -\frac{1}{d_i^1 G_1^*}\sum_{j=1}^{10} W_{im}^{6,j}(d_i^1)\frac{\left|\mathbf{\Omega}_{m,10i-10+j,k}^{(r)}\right|}{|\mathbf{\Omega}_m|},$$

$$\mathbf{A}_m^{21}(i,k) = -\frac{1}{d_i^1 G_1^*}\sum_{j=1}^{10} W_{im}^{7,j}(d_i^1)\frac{\left|\mathbf{\Omega}_{m,10i-10+j,k}^{(\theta)}\right|}{|\mathbf{\Omega}_m|},$$

$$\mathbf{A}_m^{22}(i,k) = -\frac{1}{d_i^1 G_1^*}\sum_{j=1}^{10} W_{im}^{7,j}(d_i^1)\frac{\left|\mathbf{\Omega}_{m,10i-10+j,k}^{(z)}\right|}{|\mathbf{\Omega}_m|} + \delta_{ik}\frac{G_2^*}{G_1^*},$$

$$\mathbf{A}_m^{23}(i,k) = -\frac{1}{d_i^1 G_1^*}\sum_{j=1}^{10} W_{im}^{7,j}(d_i^1)\frac{\left|\mathbf{\Omega}_{m,10i-10+j,k}^{(r)}\right|}{|\mathbf{\Omega}_m|},$$

$$\mathbf{A}_m^{31}(i,k) = -\frac{1}{2(1+\mu^*)d_i^1 G_1^*}\sum_{j=1}^{10} W_{im}^{8,j}(d_i^1)\frac{\left|\mathbf{\Omega}_{m,10i-10+j,k}^{(\theta)}\right|}{|\mathbf{\Omega}_m|},$$

$$\mathbf{A}_m^{32}(i,k) = -\frac{1}{2(1+\mu^*)d_i^1 G_1^*}\sum_{j=1}^{10} W_{im}^{8,j}(d_i^1)\frac{\left|\mathbf{\Omega}_{m,10i-10+j,k}^{(z)}\right|}{|\mathbf{\Omega}_m|},$$

$$\mathbf{A}_m^{33}(i,k) = -\frac{1}{2(1+\mu^*)d_i^1 G_1^*}\sum_{j=1}^{10} W_{im}^{8,j}(d_i^1)\frac{\left|\mathbf{\Omega}_{m,10i-10+j,k}^{(r)}\right|}{|\mathbf{\Omega}_m|} + \delta_{ik}\frac{G_2^*}{G_1^*}.$$

$$\mathbf{H}_m^1(i) = \frac{1}{d_i^1 G_1^*}\sum_{j=1}^{10} W_{im}^{6,j}(d_i^1)\frac{\left|\mathbf{\Omega}_{m,10i-10+j}^{(q)}\right|}{|\mathbf{\Omega}_m|}q_m,$$

$$\mathbf{H}_m^2(i) = \frac{1}{d_i^1 G_1^*}\sum_{j=1}^{10} W_{im}^{7,j}(d_i^1)\frac{\left|\mathbf{\Omega}_{m,10i-10+j}^{(q)}\right|}{|\mathbf{\Omega}_m|}q_m,$$

$$\mathbf{H}_m^3(i) = \frac{1}{2(1+\mu^*)d_i^1 G_1^*}\sum_{j=1}^{10} W_{im}^{8,j}(d_i^1)\frac{\left|\mathbf{\Omega}_{m,10i-10+j}^{(q)}\right|}{|\mathbf{\Omega}_m|}q_m, \tag{A4}$$

in which $i, k = 1, 2 \ldots p-1$, $\delta_{ik} = 1$ if $i = k$, and $\delta_{ik} = 0$ if $i \neq k$.

Appendix B

Examples for $J_{m,n}$ and $L_{m,n}^j$ when $p = 2$ are given as follows

$$J_{m,1} = \begin{vmatrix}1 & A_m^{12} & A_m^{13}\\ 0 & A_m^{22} & A_m^{23}\\ 0 & A_m^{32} & A_m^{33}\end{vmatrix} + \begin{vmatrix}A_m^{11} & 0 & A_m^{13}\\ A_m^{21} & 1 & A_m^{23}\\ A_m^{31} & 0 & A_m^{33}\end{vmatrix} + \begin{vmatrix}A_m^{11} & A_m^{12} & 0\\ A_m^{21} & A_m^{22} & 0\\ A_m^{31} & A_m^{32} & 1\end{vmatrix},$$

$$J_{m,2} = \begin{vmatrix}1 & 0 & A_m^{13}\\ 0 & 1 & A_m^{23}\\ 0 & 0 & A_m^{33}\end{vmatrix} + \begin{vmatrix}1 & A_m^{12} & 0\\ 0 & A_m^{22} & 0\\ 0 & A_m^{32} & 1\end{vmatrix} + \begin{vmatrix}A_m^{11} & 0 & 0\\ A_m^{21} & 1 & 0\\ A_m^{31} & 0 & 1\end{vmatrix},$$

$$J_{m,3} = \begin{vmatrix}1 & 0 & 0\\ 0 & 1 & 0\\ 0 & 0 & 1\end{vmatrix},$$

$$L_{m,1}^1 = \begin{vmatrix}H_m^1 & 0 & A_m^{13}\\ H_m^2 & 1 & A_m^{23}\\ H_m^3 & 0 & A_m^{33}\end{vmatrix} + \begin{vmatrix}H_m^1 & A_m^{12} & 0\\ H_m^2 & A_m^{22} & 0\\ H_m^3 & A_m^{32} & 1\end{vmatrix},$$

$$L_{m,2}^1 = \begin{vmatrix}H_m^1 & 0 & 0\\ H_m^2 & 1 & 0\\ H_m^3 & 0 & 1\end{vmatrix},$$

$$L^2_{m,1} = \begin{vmatrix} 1 & H^1_m & A^{13}_m \\ 0 & H^1_m & A^{23}_m \\ 0 & H^1_m & A^{33}_m \end{vmatrix} + \begin{vmatrix} A^{11}_m & H^1_m & 0 \\ A^{21}_m & H^1_m & 0 \\ A^{31}_m & H^1_m & 1 \end{vmatrix},$$

$$L^2_{m,2} = \begin{vmatrix} 1 & H^1_m & 0 \\ 0 & H^2_m & 0 \\ 0 & H^3_m & 1 \end{vmatrix},$$

$$L^3_{m,1} = \begin{vmatrix} 1 & A^{12}_m & H^1_m \\ 0 & A^{22}_m & H^2_m \\ 0 & A^{32}_m & H^3_m \end{vmatrix} + \begin{vmatrix} A^{11}_m & 0 & H^1_m \\ A^{21}_m & 1 & H^2_m \\ A^{31}_m & 0 & H^3_m \end{vmatrix},$$

$$L^3_{m,2} = \begin{vmatrix} 1 & 0 & H^1_m \\ 0 & 1 & H^2_m \\ 0 & 0 & H^3_m \end{vmatrix}.$$

Appendix B. Supplementary data

Supplementary data associated with this article can be found, in the online version, at http://dx.doi.org/10.1016/j.compstruct.2018.05.115.

References

[1] Priya S, Islam R, Dong S, Viehland D. Recent advancements in magnetoelectric particulate and laminate composites. J Electroceram 2007;19:149–66.
[2] Agarwal S, Caltun O, Sreenivas K. Magneto electric effects in BaTiO3–CoFe2O4 bulk composites. Solid State Commun 2012;152:1951–5.
[3] Qin QH, Mai Y. Crack growth prediction of an inclined crack in a half-plane thermopiezoelectric solid. Theor Appl Fract Mech 1997;26:185–91.
[4] Yu SW, Qin QH. Damage analysis of thermopiezoelectric properties: Part II. Effective crack model. Theor Appl Fract Mech 1996;25:279–88.
[5] Qin QH. General solutions for thermopiezoelectrics with various holes under thermal loading. Int J Solids Struct 2000;37:5561–78.
[6] Pan E. Exact solution for simply supported and multilayered magneto-electro-elastic plates. J Appl Mech 2001;68:608–18.
[7] Qin QH, Yu SW. An arbitrarily-oriented plane crack terminating at the interface between dissimilar piezoelectric materials. Int J Solids Struct 1997;34:581–90.
[8] Ke L-L, Wang Y-S. Free vibration of size-dependent magneto-electro-elastic nanobeams based on the nonlocal theory. Physica E 2014;63:52–61.
[9] Vel SS, Mewer R, Batra R. Analytical solution for the cylindrical bending vibration of piezoelectric composite plates. Int J Solids Struct 2004;41:1625–43.
[10] Qin QH, Ye JQ. Thermoelectroelastic solutions for internal bone remodeling under axial and transverse loads. Int J Solids Struct 2004;41:2447–60.
[11] Liu X, Wang Q, Quek S. Analytical solution for free vibration of piezoelectric coupled moderately thick circular plates. Int J Solids Struct 2002;39:2129–51.
[12] Ma L-H, Ke L-L, Wang Y-Z, Wang Y-S. Wave propagation in magneto-electro-elastic nanobeams via two nonlocal beam models. Physica E 2017;86:253–61.
[13] Wu CP, Lu YC. A modified Pagano method for the 3D dynamic responses of functionally graded magneto-electro-elastic plates. Compos Struct 2009;90:363–72.
[14] Ke LL, Wang YS, Yang J, Kitipornchai S. Free vibration of size-dependent magneto-electro-elastic nanoplates based on the nonlocal theory. Acta Mech Sin 2014;30:516–25.
[15] Milazzo A, Orlando C, Alaimo A. An analytical solution for the magneto-electro-elastic bimorph beam forced vibrations problem. Smart Mater Struct 2009;18:085012.
[16] Ke L-L, Wang Y-S, Yang J, Kitipornchai S. The size-dependent vibration of embedded magneto-electro-elastic cylindrical nanoshells. Smart Mater Struct 2014;23:125036.
[17] Jiang J, Zhu J, Chen W. Dispersion curves of magneto-electro-elastic imperfect cylinders filled with fluid. Math Mech Solids 2017.
[18] Zhou Y, Chen W, Lü C. Semi-analytical solution for orthotropic piezoelectric laminates in cylindrical bending with interfacial imperfections. Compos Struct 2010;92:1009–18.
[19] Fang Q, Feng H, Liu Y. Electroelastic interaction between piezoelectric screw dislocation and circularly layered inclusion with imperfect interfaces. Appl Math Mech 2013;34:45–62.
[20] Wang X, Zhong Z. Three-dimensional solution of smart laminated anisotropic circular cylindrical shells with imperfect bonding. Int J Solids Struct 2003;40:5901–21.
[21] Bayat J, Ayatollahi M, Bagheri R. Fracture analysis of an orthotropic strip with imperfect piezoelectric coating containing multiple defects. Theor Appl Fract Mech 2015;77:41–9.
[22] López-Realpozo J, Rodríguez-Ramos R, Guinovart-Díaz R, Bravo-Castillero J, Camacho-Montes H, Espinosa-Almeyda Y, et al. Analysis of mechanical and electrical imperfect contacts in piezoelectric composites. Mech Res Commun 2017.
[23] Otero J, Rodríguez-Ramos R, Monsivais G, Stern C, Martínez R, Dario R. Interfacial waves between two magneto-electro-elastic half-spaces with magneto-electro-mechanical imperfect interface. Philos Mag Lett 2014;94:629–38.
[24] Rodriguez-Ramos R, Guinovart-Diaz R, Lopez-Realpozo JC, Bravo-Castillero J, Sabina FJ, Lebon F, et al. Characterization of piezoelectric composites with mechanical and electrical imperfect contacts. J Compos Mater 2016;50:1603–25.
[25] Meshgin P, Choi K-K, Taha MMR. Experimental and analytical investigations of creep of epoxy adhesive at the concrete–FRP interfaces. Int J Adhes Adhes 2009;29:56–66.
[26] Bardenhagen SG, Stout MG, Gray GT. Three-dimensional, finite deformation, viscoplastic constitutive models for polymeric materials. Mech Mater 1997;25:235–53.
[27] Woo E, Seferis J, Schaffnit R. Viscoelastic characterization of high performance epoxy matrix composites. Polym Compos 1991;12:273–80.
[28] Yang M, Zhao Y, Zhang N. Creep behavior of epoxy-bonded anchor system. Int J Rock Mech Min Sci 2014;67:96–103.
[29] Chen J, Liu L, Liu Y, Leng J. Thermoviscoelastic shape memory behavior for epoxy-shape memory polymer. Smart Mater Struct 2014;23:055025.
[30] Qin QH, Yang QS. Macro-micro theory on multifield coupling behavior of heterogenous materials. Beijing: Higher Education Press and Springer; 2008.
[31] Qin QH. Green's function and boundary elements of multifield materials. Oxford: Elsevier; 2007.
[32] Arzoumanidis G, Liechti K. Linear viscoelastic property measurement and its significance for some nonlinear viscoelasticity models. Mech Time-Depend Mater 2003;7:209–50.
[33] Galuppi L, Royer-Carfagni G. Laminated beams with viscoelastic interlayer. Int J Solids Struct 2012;49:2637–45.
[34] Souchek J, Li LY. Structure of rings of functions with Riemann Stieltjes convolution products. J Math Anal Appl 1973;41:468–77.
[35] Wang X, Pan E. Interaction between a screw dislocation and a viscoelastic piezoelectric bimaterial interface. Int J Solids Struct 2008;45:245–57.
[36] Wang X, Sudak L. A piezoelectric screw dislocation interacting with an imperfect piezoelectric bimaterial interface. Int J Solids Struct 2007;44:3344–58.
[37] Xu YP, Zhou D, Cheung YK. Elasticity solution of clamped-simply supported beams with variable thickness. Appl Math Mech 2008;29:279–90.